

General time-dependent formulation of quantum scattering theory

Stuart C. Althorpe*

Department of Chemistry, University of Exeter, Stocker Road, Exeter EX4 4QD, United Kingdom

(Received 15 November 2003; published 2 April 2004)

We derive and explain the key ideas behind a time-dependent formulation of quantum scattering theory, applicable generally to systems with a finite-range scattering potential. The scattering is initiated and probed by plane wave packets, which are localized just outside the range of the potential. The asymptotic limits of conventional scattering theory (initiation in the remote past; detection in the remote future) are not taken. Instead, the differential cross section (DCS) is obtained by projecting the scattered wave packet onto the probe plane wave packets. The projection also yields a time-dependent version of the DCS. Cuts through the wave packet, just as it exits the scattering potential, yield time-dependent and time-independent angular distributions that give a close-up picture of the scattering which complements the DCS. We have previously applied the theory to interpret experimental cross sections of chemical reactions [e.g., S. C. Althorpe, F. Fernández-Alonso, B. D. Bean, J. D. Ayers, A. E. Pomerantz, R. N. Zare, and E. Wrede, *Nature (London)* **416**, 67 (2002)]. This paper gives the derivation of the theory, and explains its relation to conventional scattering theory. For clarity, the derivation is restricted to spherical-particle scattering, though it may readily be extended to general multichannel systems. We illustrate the theory using a simple application to hard-sphere scattering.

DOI: 10.1103/PhysRevA.69.042702

PACS number(s): 34.10.+x, 34.50.-s, 34.50.Lf, 34.80.-i

I. INTRODUCTION

In recent calculations on chemically reactive scattering [1–5], we have devised an approach for interpreting differential cross sections (DCS) in terms of the scattering of a plane wave packet. The plane wave packet is placed at the shortest distance from the scattering center at which the interaction potential can be neglected, and contains a wide enough spread of momenta to localize the initial positions of the collision partners. The ensuing time evolution of this wave packet visualizes the dynamics of the collision, on and close to the scattering potential. The packet maps directly onto the DCS, via a simple transformation [2], and this mapping is often able to decompose the DCS into contributions from different scattering mechanisms.

To our surprise, this intuitive approach seems not to have been applied elsewhere in the quantum scattering literature. Textbook derivations [6–8] often employ a plane wave packet, but they assume that the spread of momenta in the packet is very narrow, that the initial wave packet is prepared in the remote past, and that the scattering is detected in the remote future. These assumptions result in the standard, time-independent formulation of quantum scattering theory, which is essentially a plane wave packet description, on the length and time scale of an experiment (in which the projectiles and the detector are a very large distance away from the scattering center). Our approach, by contrast, gives a plane wave packet description on the length and time scale of the collision. This “close-up” picture of the scattering maps onto the “distant” picture given by the DCS, through projections of the time-evolving wave packet onto a series of fixed plane wave packets, each pointing in a desired scattering direction

[2]. The analogous mapping has been used for some years in electromagnetic wave scattering theory [9,10], but it seems not to have been used in quantum scattering before our work on chemical reactions [1–5]. The latter did not derive the approach formally, but arrived at it on the basis of physical intuition.

It may be useful, therefore, to present a derivation of our plane wave packet approach, since it is not restricted to chemical reactions, and might profitably be applied in other branches of quantum scattering. In this paper, we derive the approach for the simplest case of spherical-particle scattering. The straightforward extension to multichannel scattering will be presented in a later paper. The aim here is to illustrate the main ideas behind the approach, including the simple mapping between the wave packet and the DCS. To avoid confusion, we emphasize that we are dealing here with the use of wave packets as an *interpretational tool*. We do not discuss the other use of wave packets in quantum scattering theory, namely as a powerful numerical technique for solving the Schrödinger equation [11–17]. Such techniques provide a natural way of implementing the approach of this paper, but, as we explain below, standard time-independent methods of solving the Schrödinger equation can also be used.

In Sec. II, we summarize the key results of the plane wave packet approach. In Sec. III we derive these results by making a partial-wave analysis. In Sec. IV, we illustrate the theory by calculating time-evolving plane wave packets, and angular distributions, for the simple example of hard-sphere scattering. In Sec. V, we discuss how to apply the approach to calculations that use time-independent methods of solving the Schrödinger equation. Section VI concludes the paper.

II. PLANE WAVE PACKET FORMULATION OF QUANTUM SCATTERING

In this section, we summarize the key steps in our plane wave packet approach of quantum scattering theory, most of

*Email address: s.c.althorpe@ex.ac.uk;

URL: <http://www.ex.ac.uk/~scalthor>

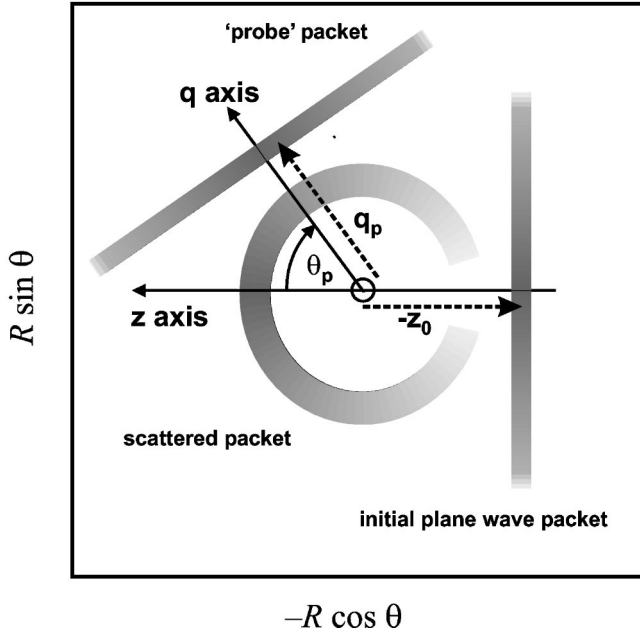


FIG. 1. Schematic picture of the plane wave packet approach (adapted from Fig. 1 of Ref. [2]), showing a $\phi=0$ cut through the 3D space in which the particle scatters. The initial plane wave packet is placed at the shortest distance $|z_0|$ from the origin at which the scattering potential can be neglected, and is traveling in the direction of the z axis. The DCS is obtained by projecting the scattered wave packet onto a series of fixed, plane-wave probe packets. One such probe packet is shown, pointing in the direction $\theta=\theta_p$.

which have been applied previously by us [1–5], without proof. We define the initial wave packet, the close-up angular distributions, and the mapping between the time-evolving wave packet and the DCS. These results will be derived in Sec. III. For simplicity of presentation, we consider only spherical-particle scattering, although the theory discussed in this paper is easy to extend to general, multichannel scattering.

A. The time-dependent wave packet

The scattering of the particle is described in terms of the usual spherical polar coordinates $\mathbf{R}=(R, \theta, \phi)$, of which R is the distance of the particle from the scattering center, θ is the scattering angle with respect to the initial approach direction along the z axis, and ϕ is the azimuthal angle. Since we are treating spherical-particle scattering, the wave function is symmetric about ϕ , and the angle ϕ will often be dropped. We assume that the scattering potential $V(R)$ has a finite range and may be neglected for $R>R_0$.

At the initial time $t=0$, the system is described by a plane wave packet [2]

$$\chi(\mathbf{R}|\bar{k}_0, z_0|0) = A(z - z_0)e^{i\bar{k}_0 z}. \quad (1)$$

The packet is traveling in the direction of the positive z axis, as shown schematically in Fig. 1. The envelope $A(z - z_0)$ is chosen so as to localize the packet about a negative z distance, as close to the scattering center as possible without the

packet significantly overlapping the potential. The momentum composition of the packet is given by

$$A(k|\bar{k}_0, z_0) = \frac{1}{2\pi} \int_{-\infty}^{\infty} e^{-ikz} \chi(\mathbf{R}|\bar{k}_0, z_0|0) dz \quad (2)$$

and the average momentum in the positive z direction is $\bar{k}_0\hbar$. The dynamics of the particle at $t>0$ is described by the time-dependent wave packet

$$\chi(\mathbf{R}|\bar{k}_0, z_0|t) = e^{-i\hat{H}t/\hbar} \chi(\mathbf{R}|\bar{k}_0, z_0|0), \quad (3)$$

where \hat{H} is the Hamiltonian. To separate the scattered part of the wave packet from the unscattered part, we define the wave packet

$$\chi^{\text{OUT}}(\mathbf{R}|\bar{k}_0, z_0|t) = \chi(\mathbf{R}|\bar{k}_0, z_0|t) - \chi^{\text{PW}}(\mathbf{R}|\bar{k}_0, z_0|t), \quad (4)$$

where $\chi^{\text{PW}}(\mathbf{R}|\bar{k}_0, z_0|t)$ is given by

$$\chi^{\text{PW}}(\mathbf{R}|\bar{k}_0, z_0|t) = e^{-i\hat{H}_0 t/\hbar} \chi(\mathbf{R}|\bar{k}_0, z_0|0) \quad (5)$$

and \hat{H}_0 is the free particle Hamiltonian.

To relate the time-dependent wave packet to the time-independent wave function $\Psi(\mathbf{R}|E)$ of conventional scattering theory [6–8], we take the Fourier transform over t to obtain

$$\xi(\mathbf{R}|\bar{k}_0, z_0|E) = \frac{1}{2\pi\hbar} \int_0^{\infty} e^{iEt/\hbar} \chi(\mathbf{R}|\bar{k}_0, z_0|t) dt. \quad (6)$$

The time-independent wave function $\xi(\mathbf{R}|\bar{k}_0, z_0|E)$ is often called the “time-independent wave packet” (TIWP) [18], and is the solution of an inhomogeneous form of the time-independent Schrödinger equation. One may show (Appendix A) that $\Psi(\mathbf{R}|E)$ is related to $\xi(\mathbf{R}|\bar{k}_0, z_0|E)$ by

$$\Psi(\mathbf{R}|E) = \frac{\hbar^2 k}{mA(k|\bar{k}_0, z_0)} \xi(\mathbf{R}|\bar{k}_0, z_0|E), \quad (7)$$

where m is the mass of the particle, and $\Psi(\mathbf{R}|E)$ satisfies the usual scattering boundary condition [6–8],

$$\Psi(\mathbf{R}|E) \rightarrow e^{ikz} + \frac{f(\theta, E)}{R} e^{ikR} \quad \text{as } R \rightarrow \infty. \quad (8)$$

Strictly speaking, Eq. (7) breaks down when describing the incoming part of the wave function at values of $z < z_0$ (see Appendix A). This drawback is only minor, since the incoming part of $\Psi(\mathbf{R}|E)$ is of course just e^{ikz} for $z < z_0$.

The goal of most scattering calculations is the scattering amplitude $f(\theta, E)$ which yields the DCS,

$$\frac{d\sigma}{d\Omega}(\theta, E) = |f(\theta, E)|^2. \quad (9)$$

The textbook [6–8] route to obtaining $f(\theta, E)$ from a plane wave packet is to take the limits $z_0 \rightarrow -\infty$ and $A(k|\bar{k}_0, z_0) \rightarrow \delta(k - \bar{k}_0)$, and then to obtain the scattering amplitude of the wave packet in the limit $t \rightarrow \infty$. However, as we discuss be-

low, one does not need to take these limits, in order to obtain $f(\theta, E)$ from the wave packet. We need the packet only up to such a time t_{\max} at which $\chi^{\text{OUT}}(\mathbf{R}|\bar{k}_0, z_0|t)$ has escaped the scattering potential (i.e., is confined to $R > R_0$). (In a numerical calculation, the wave packet would be absorbed or damped at some R slightly greater than R_0 .) The wave packet $\chi(\mathbf{R}|\bar{k}_0, z_0|t)$ thus describes the dynamics of the scattering on the length and time scale of the collision.

B. The close-up angular distributions

It is useful to obtain the angular distribution of the wave packet just as it exits the scattering potential. We therefore introduce the close-up angular distributions $\tilde{\sigma}(\theta, t)$ and $\tilde{\sigma}(\theta, E)$, which are time-dependent and time-independent angular distributions, taken over a sphere which just encloses the scattering potential. These distributions give a local picture of the scattering, which separates out parts of the packet that have scattered from different parts of the potential. The information in the time-independent angular distribution $\tilde{\sigma}(\theta, E)$ therefore complements the information in the (time-independent) DCS.

To obtain the time-dependent distribution $\tilde{\sigma}(\theta, t)$, we take a cut through the wave packet at the angle θ , then calculate the flux of the wave packet normal to a sphere that just encloses the scattering potential. We do this by projecting the packet onto a radial “probe” packet $\chi(R|\bar{k}_p, R_p)/R$, which is localized about $R=R_p > R_0$, and contains a spread of momenta pointing radially outwards, with average momentum $\hbar\bar{k}_p$. The use of such a probe or “test” packet is known [19] to be equivalent to acting with the radial flux operator [6–8]. The spread of momenta in $\chi(R|\bar{k}_p, R_p)$ must be chosen so as to enclose the momenta contained in $A(k|\bar{k}_0, z_0)$ of Eq. (2). This procedure yields the close-up scattering amplitude

$$\tilde{f}(\theta, t) = \langle \chi(\bar{k}_p, R_p) | \chi^{\text{OUT}}(\theta|\bar{k}_0, z_0|t) \rangle, \quad (10)$$

where we have omitted from $\chi(R|\bar{k}_p, R_p)$ and $\chi^{\text{OUT}}(\mathbf{R}|\bar{k}_0, z_0|t)$ the variable (R) over which we have integrated. (This convention is used throughout the paper.) The close-up, time-dependent angular distribution is then

$$\tilde{\sigma}(\theta, t) = |\tilde{f}(\theta, t)|^2. \quad (11)$$

To obtain the corresponding time-independent distribution, we take the time-to-energy Fourier transform of $\tilde{f}(\theta, t)$ to obtain

$$\tilde{g}(\theta, E) = \frac{1}{2\pi\hbar} \int_0^\infty e^{iEt/\hbar} \tilde{f}(\theta, t) dt, \quad (12)$$

which gives the close-up, time-independent angular distribution

$$\tilde{\sigma}(\theta, E) = |\tilde{g}(\theta, E)|^2. \quad (13)$$

It is important to realize that the close-up angular distributions $\tilde{\sigma}(\theta, t)$ and $\tilde{\sigma}(\theta, E)$ are *not* differential cross sections. If R_p were allowed to tend to infinity then $\tilde{\sigma}(\theta, E)$ would tend

to the differential cross section (multiplied by an energy factor). However, the aim is to keep R_p as small as possible, so that $\tilde{\sigma}(\theta, t)$ and $\tilde{\sigma}(\theta, E)$ can distinguish between scattering from different parts of the potential. Integrating $\tilde{\sigma}(\theta, E)$ over the sphere does not yield the integral cross section, since some of the flux that would be traveling radially outwards at large R_p is traveling tangentially to the sphere at finite R_p . It seems that the close-up distributions, which reveal information that complements the DCS, have not been used previously in quantum scattering calculations. As we show in Sec. III C, the time-independent distribution $\tilde{\sigma}(\theta, E)$ is readily obtained from the S matrix, and hence from a standard scattering calculation (e.g., using the coupled-channel method).

C. Mapping the wave packet onto the DCS

The main idea behind our approach is that it is simple to map the wave packet, which describes the scattering on and close to the potential surface, onto the DCS (which describes the scattering from a very large distance). Of course, one could obtain the DCS from the wave packet via an indirect route, by extracting the partial-wave S -matrix elements [12]. However, what we propose is a direct mapping, which allows features in the DCS to be explained in terms of events in the dynamics of the wave packet.

The mapping is analogous to a technique which, in electromagnetic wave scattering, is called the “near-field to far-field” transformation [9,10]. It is essentially an application of Newton’s first law to the motion of the wave packet for $R > R_0$, which projects out the component of the packet whose momentum vector points in the direction of a given angle θ , and which will therefore scatter into this angle in the limit $R \rightarrow \infty$. One could use a flux operator to apply the mapping or equivalently, as we have done [2], one can project onto probe packets. The probe packets are a set of plane wave packets, held tangentially to a sphere of radius R_p . Each packet points in a desired scattering direction θ_p ; one such probe packet is illustrated schematically in Fig. 1. Using a similar notation to Eq. (1), we write these packets as

$$\chi(\mathbf{R}|\theta_p, \bar{k}_p, q_p) = A(q - q_p) e^{i\bar{k}_p q}. \quad (14)$$

The envelope function $A(q - q_p)$ is chosen such that $\chi(\mathbf{R}|\theta_p, \bar{k}_p, q_p)$ is localized about the distance $q = q_p$ along the q axis (a vector pointing in the direction of θ_p ; see Fig. 1). The spread of $\hbar|k|$ in $\chi(\mathbf{R}|\theta_p, \bar{k}_p, q_p)$ must enclose the spread of $\hbar|k|$ in the initial wave packet $\chi(\mathbf{R}|\bar{k}_0, z_0|0)$. Projecting onto $\chi(\mathbf{R}|\theta_p, \bar{k}_p, q_p)$ effectively “captures” all those parts of the packet which, in the limit $R \rightarrow \infty$, will scatter into $\theta = \theta_p$.

The projection yields the time-dependent scattering amplitude

$$f(\theta_p, t) = \langle \chi(\theta_p, \bar{k}_p, q_p) | \chi^{\text{OUT}}(\bar{k}_0, z_0|t) \rangle, \quad (15)$$

from which we obtain (dropping the p subscripts) the “time-dependent differential cross section”

$$\frac{d\sigma}{d\Omega}(\theta, t) = |f(\theta, t)|^2. \quad (16)$$

The time-to-energy Fourier transform of $f(\theta, t)$ yields a time-independent scattering amplitude

$$g(\theta, E) = \frac{1}{2\pi\hbar} \int_0^\infty e^{iEt/\hbar} f(\theta, t) dt. \quad (17)$$

We will demonstrate below (Sec. III D) that $g(\theta, E)$ is related to $f(\theta, E)$ by

$$f(\theta, E) = \frac{g(\theta, E)}{F(\bar{k}_0, z_0, \bar{k}_p, q_p | E)}, \quad (18)$$

where the energy filter $F(\bar{k}_0, z_0, \bar{k}_p, q_p | E)$ is

$$F(\bar{k}_0, z_0, \bar{k}_p, q_p | E) = \frac{4\pi^2 im}{k^2 \hbar^2} A(k | \bar{k}_0, z_0) A(k | \bar{k}_p, q_p)^*. \quad (19)$$

Hence, the mapping between the wave packet $\chi^{\text{OUT}}(\mathbf{R} | \bar{k}_0, z_0 | t)$ and the DCS involves simply the projection onto the probe packets, followed by a Fourier transform. A quantitative picture of the mapping, which helps to show which parts of the wave packet map onto which features in the DCS, is given by the time-dependent DCS $d\sigma/d\Omega(\theta, t)$ [Eq. (16)]. Strictly speaking, $d\sigma/d\Omega(\theta, t)$ should not be called a ‘‘cross section,’’ since it is not a ratio of scattered flux to incoming flux, and does not in general have units of area [20]. However, the name and notation seem appropriate given the close relation between $d\sigma/d\Omega(\theta, t)$ and the (time-independent) DCS.

III. PARTIAL-WAVE ANALYSIS

In this section we derive the results summarized in Sec. II, including the mapping between $\chi^{\text{OUT}}(\mathbf{R} | \bar{k}_0, z_0 | t)$ and $f(\theta, E)$, by making a partial-wave analysis. This analysis also clarifies the relation with conventional scattering theory, and gives a practical way of implementing the plane wave packet approach numerically (see Sec. IV). In electromagnetic scattering theory, the analogous relations have been derived [9,10] by an explicit application of Green’s theorem. Here we are effectively following the same route, since the well-known properties of the partial-wave series that we exploit are themselves a consequence of Green’s theorem.

A. Expanding the time-dependent wave packet

The derivation is based on the well-known expansion

$$e^{ikz} = \frac{1}{kR} \sum_{l=0}^{\infty} (2l+1) i^l \hat{j}_l(kR) P_l(\cos \theta), \quad (20)$$

where $P_l(\cos \theta)$ are Legendre polynomials, $\hat{j}_l(kR)$ are Riccati-Bessel functions satisfying

$$\hat{j}_l(kR) \rightarrow \sin(kR - l\pi/2), \quad (21)$$

and l is the (orbital) angular momentum of the scattering particle.

Application of Eq. (20) to the time-evolving wave packet $\chi(\mathbf{R} | \bar{k}_0, z_0 | t)$ yields

$$\chi(\mathbf{R} | \bar{k}_0, z_0 | t) = \frac{1}{R} \sum_{l=0}^{\infty} i^l (2l+1) P_l(\cos \theta) \chi_l(R | \bar{k}_0, z_0 | t). \quad (22)$$

Each of the partial wave packets $\chi_l(R | \bar{k}_0, z_0 | t)$ satisfies

$$\chi_l(R | \bar{k}_0, z_0 | t) = e^{-i\hat{H}_l t/\hbar} \chi_l(R | \bar{k}_0, z_0 | 0), \quad (23)$$

where \hat{H}_l is the Hamiltonian

$$\hat{H}_l = -\frac{\hbar^2}{2m} \frac{d^2}{dR^2} + \frac{l(l+1)\hbar^2}{2mR^2} + V(R) \quad (24)$$

and $\chi_l(R | \bar{k}_0, z_0 | 0)$ is the partial-wave component of the initial plane wave packet $\chi(\mathbf{R} | \bar{k}_0, z_0 | 0)$. Using Eq. (2) to write the latter as

$$\chi(\mathbf{R} | \bar{k}_0, z_0 | 0) = \int_{-\infty}^{\infty} e^{ikz} A(k | \bar{k}_0, z_0) dk \quad (25)$$

and expanding e^{ikz} using Eq. (20), yields

$$\chi_l(R | \bar{k}_0, z_0 | 0) = \int_{-\infty}^{\infty} \hat{j}_l(kR) \frac{A(k | \bar{k}_0, z_0)}{k} dk. \quad (26)$$

This equation gives the general form of $\chi_l(R | \bar{k}_0, z_0 | 0)$ for a given momentum envelope $A(k | \bar{k}_0, z_0)$. To our knowledge, the integral over k cannot be evaluated analytically for $l > 0$, for any simple choice of $A(k | \bar{k}_0, z_0)$ (such as a Gaussian), and hence the form of the $\chi_l(R | \bar{k}_0, z_0 | 0)$ must be investigated numerically. This is done in Sec. IV A. Here, we point out some basic properties of the $\chi_l(R | \bar{k}_0, z_0 | 0)$. These packets superpose to give the initial plane wave packet $\chi(\mathbf{R} | \bar{k}_0, z_0 | 0)$, and hence they are localized around $R \geq |z_0|$, and are incoming waves (traveling in the direction of decreasing R). Now, the function $\hat{j}_l(kR)$ is a linear combination of incoming and outgoing waves

$$\hat{j}_l(kR) = \frac{1}{2i} [\hat{h}_l^+(kR) - \hat{h}_l^-(kR)] \quad (27)$$

and so the effect of integrating over $A(k | \bar{k}_0, z_0)$ is to pick out the incoming component $\hat{h}_l^-(kR)$, and localize it about a positive value of R . The contribution of the outgoing wave to $\chi_l(R | \bar{k}_0, z_0 | 0)$ is negligible, since integrating over $A(k | \bar{k}_0, z_0)$ would localize it about a negative value of R (and $R \geq 0$). For $l=0$, the integral in Eq. (26) is simply a Fourier transform, which yields a $\chi_0(R | \bar{k}_0, z_0 | 0)$ that is centered about $R = |z_0|$. From Eqs. (25) and (26), the distribution of momenta in $\chi_0(R | \bar{k}_0, z_0 | 0)$ is $1/k$ times the distribution in the plane wave packet $\chi(\mathbf{R} | \bar{k}_0, z_0 | 0)$. Higher values of l correspond to higher impact parameters and hence, from simple geometry we expect that, as l increases, the value of R about which

$\chi_l(R|\bar{k}_0, z_0|0)$ is centered moves further out, and the width of $\chi_l(R|\bar{k}_0, z_0|0)$ increases.

We also define the partial wave packets $\chi_l^{\text{PW}}(R|\bar{k}_0, z_0|t)$ and $\chi_l^{\text{OUT}}(R|\bar{k}_0, z_0|t) = \chi_l(R|\bar{k}_0, z_0|t) - \chi_l^{\text{PW}}(R|\bar{k}_0, z_0|t)$, which are the analogous partial-wave components of $\chi^{\text{OUT}}(\mathbf{R}|\bar{k}_0, z_0|t)$ and $\chi^{\text{PW}}(\mathbf{R}|\bar{k}_0, z_0|t)$ of Eqs. (4) and (5). Hence, $\chi_l^{\text{PW}}(R|\bar{k}_0, z_0|t)$ describes the free evolution of an initial partial wave packet $\chi_l(R|\bar{k}_0, z_0|0)$, subject to a Hamiltonian \hat{H}_l of Eq. (24) in which $V(R)$ is zero.

B. Relation to the time-independent wave function

The next step is to relate the partial wave packets $\chi_l(R|\bar{k}_0, z_0|t)$ to the partial-wave components $\Psi_l(R|E)$ of the time-independent wave function $\Psi(\mathbf{R}|E)$, and thus to the S -matrix elements $S_l(E)$. The $\Psi_l(R|E)$ are defined [6–8] by the expansion

$$\Psi(\mathbf{R}|E) = \frac{1}{kR} \sum_{l=0}^{\infty} (2l+1) i^l P_l(\cos \theta) \Psi_l(R|E) \quad (28)$$

and satisfy the boundary conditions

$$\Psi_l(R|E) \rightarrow \frac{i}{2} [\hat{h}_l^-(kR) - \hat{h}_l^+(kR) S_l(E)], \quad (29)$$

where $S_l(E)$ are elements of the S matrix. Proceeding as in Sec. II A, we define the TIWP partial-wave components

$$\xi_l(R|\bar{k}_0, z_0|E) = \frac{1}{2\pi\hbar} \int_0^{\infty} e^{iEt/\hbar} \chi_l(R|\bar{k}_0, z_0|t) dt, \quad (30)$$

which satisfy

$$\xi(\mathbf{R}|\bar{k}_0, z_0|E) = \frac{1}{R} \sum_{l=0}^{\infty} i^l (2l+1) P_l(\cos \theta) \xi_l(R|\bar{k}_0, z_0|E). \quad (31)$$

We then substitute Eqs. (28) and (31) into Eq. (7) and use the orthogonality of the $P_l(\cos \theta)$ to obtain

$$\Psi_l(R|E) = \frac{\hbar^2 k^2}{mA(k|\bar{k}_0, z_0)} \xi_l(R|\bar{k}_0, z_0|E). \quad (32)$$

The same relation holds between $\xi_l^{\text{PW}}(R|\bar{k}_0, z_0|E)$ and $\Psi_l^{\text{PW}}(R|E) [= \hat{j}_l(kR)]$, and between $\xi_l^{\text{OUT}}(R|\bar{k}_0, z_0|E)$ and $\Psi_l^{\text{OUT}}(R|E)$. The latter is given by

$$\Psi_l^{\text{OUT}}(R|E) = -\frac{i}{2} \hat{h}_l^+(kR) [S_l(E) - 1] \quad \text{for } R > R_0. \quad (33)$$

Thus Eqs. (22) and (30)–(33) can be used to extract the S -matrix elements $S_l(E)$ from the time-dependent wave packet. These yield the scattering amplitude $f(\theta, E)$, and hence the DCS, through the well-known expression

$$f(\theta, E) = \frac{1}{2ik} \sum_{l=0}^{\infty} (2l+1) P_l(\cos \theta) [S_l(E) - 1]. \quad (34)$$

As mentioned earlier, this gives us an alternative, indirect route, of obtaining the DCS from the wave packet. Unlike the projection onto probe packets, however, this indirect route does not allow one to map events in the dynamics of the wave packet onto features in the DCS.

C. Expanding the close-up angular distributions

Before deriving the mapping of the wave packet onto the DCS, it is useful to expand the close-up angular distributions $\bar{\sigma}(\theta, t)$ and $\bar{\sigma}(\theta, E)$ of Sec. II B, in terms of the S -matrix elements $S_l(E)$. Substituting Eq. (22) into Eq. (10) yields the expansion

$$\tilde{f}(\theta, t) = \sum_{l=0}^{\infty} i^l (2l+1) P_l(\cos \theta) \langle \chi(\bar{k}_p, R_p) | \chi_l^{\text{OUT}}(\bar{k}_0, z_0|t) \rangle. \quad (35)$$

Substituting Eqs. (30) and (31) into Eq. (12) yields

$$\tilde{g}(\theta, E) = \sum_{l=0}^{\infty} i^l (2l+1) P_l(\cos \theta) \langle \chi(\bar{k}_p, R_p) | \xi_l^{\text{OUT}}(\bar{k}_0, z_0|E) \rangle. \quad (36)$$

If we extract $S_l(E)$ from $\xi_l^{\text{OUT}}(\bar{k}_0, z_0|E)$ using Eqs. (32) and (33), then Eq. (36) becomes

$$\tilde{g}(\theta, E) = \frac{-im\pi A(k|\bar{k}_0, z_0)}{k^2 \hbar^2} \sum_{l=0}^{\infty} i^l (2l+1) P_l(\cos \theta) A_l(k|\bar{k}_p, R_p) \times [S_l(E) - 1], \quad (37)$$

where

$$A_l(k|\bar{k}_p, R_p) = \frac{1}{2\pi} \int_0^{\infty} [\chi(R|\bar{k}_p, R_p)]^* \hat{h}_l^+(kR) dR. \quad (38)$$

Comparison of Eq. (37) with Eq. (34) shows that it is the l -dependent momentum envelopes $A_l(k|\bar{k}_p, R_p)$ which ensure that the close-up angular distribution $\tilde{g}(\theta, E)$ is different from the asymptotic angular distribution $f(\theta, E)$. In the limit that the radius of the sphere $R_p \rightarrow \infty$, the envelopes satisfy

$$A_l(k|\bar{k}_p, R_p) \rightarrow A_0(k|\bar{k}_p, R_p) i^{-l}, \quad (39)$$

which ensures that $\tilde{g}(\theta, E)$ tends to $f(\theta, E)$, multiplied by an energy filter. Equation (37) is very useful, because it gives us a way of obtaining $\tilde{g}(\theta, E)$, and hence $\bar{\sigma}(\theta, E)$ and $\bar{\sigma}(\theta, t)$, from the $S_l(E)$.

D. Mapping the wave packet onto the DCS

To complete the derivation of the mapping of the wave packet onto the DCS, we need to expand the plane wave probe packets $\chi(\mathbf{R}|\theta_p, \bar{k}_p, q_p)$ of Eq. (14). Using the standard

partial wave expansion [6–8] for a plane wave function traveling in the direction of θ_p , we obtain

$$\chi(\mathbf{R}|\theta_p, \bar{k}_p, q_p) = \frac{4\pi}{R} \sum_{l=0}^{\infty} \sum_{m=-l}^l i^l Y_{lm}^*(\theta_p, 0) Y_{lm}(\theta, \phi) \chi_l(R|\bar{k}_p, q_p). \quad (40)$$

Each function $\chi_l(R|\bar{k}_p, q_p)$ is a partial wave probe packet, and has the same form as the partial-wave initial packets, $\chi_l(R|\bar{k}_0, z_0|0)$ of Eq. (26). We expand the projection onto the probe packets, given in Eq. (15), by expanding $\chi(\mathbf{R}|\bar{k}_0, z_0|t)$ and $\chi(\mathbf{R}|\theta_p, \bar{k}_p, q_p)$ using Eqs. (22) and (40), and integrating over θ , to obtain

$$f(\theta_p, t) = 4\pi \sum_{l=0}^{\infty} (2l+1) P_l(\cos \theta_p) \langle \chi_l(\bar{k}_p, q_p) | \chi_l^{\text{OUT}}(\bar{k}_0, z_0|t) \rangle. \quad (41)$$

The Fourier transform of this expression yields

$$g(\theta, E) = 4\pi \sum_{l=0}^{\infty} (2l+1) P_l(\cos \theta) \langle \chi_l(\bar{k}_p, q_p) | \xi_l^{\text{OUT}}(\bar{k}_0, z_0|E) \rangle \quad (42)$$

(where we have dropped the p subscript). From Eqs. (32) and (33), the projection on the right-hand side is equal to

$$\begin{aligned} \langle \chi_l(\bar{k}_p, q_p) | \xi_l^{\text{OUT}}(\bar{k}_0, z_0|E) \rangle &= \frac{-im}{2k^2 \hbar^2} A(k|\bar{k}_0, z_0) [S_l(E) - 1] \\ &\times \int_0^{\infty} \chi_l^*(R|\bar{k}_p, q_p) \hat{h}_l^+(kR) dR. \end{aligned} \quad (43)$$

One can show (Appendix B) that the integral over R is independent of l , and is equal to $i\pi A^*(k|\bar{k}_p, q_p)/k$. The expansion of $g(\theta, E)$ can therefore be written

$$g(\theta_p, E) = F(\bar{k}_0, z_0, \bar{k}_p, q_p|E) \times \left\{ \frac{1}{2ik} \sum_{l=0}^{\infty} (2l+1) P_l(\cos \theta_p) [S_l(E) - 1] \right\}, \quad (44)$$

where the energy filter $F(\bar{k}_0, z_0, \bar{k}_p, q_p|E)$ is as defined in Eq. (19). The term in brackets is equal to $f(\theta, E)$ [see Eq. (34)], and so Eq. (44) is equivalent to Eq. (18).

This completes the derivation of the mapping of the wave packet onto the DCS. The plane wave packet approach given in Sec. II (and applied without proof in previous work [1–5]) is therefore a rigorous formulation of quantum scattering theory, which is consistent with conventional scattering theory. Both formulations yield the same final result (the time-independent DCS), but by different routes. The plane wave packet approach obtains the DCS by projecting the wave packet onto probe packets; conventional scattering theory by summing the partial-wave S -matrix elements.

Note that the formulas of this section and Sec. II give several different (but equivalent) ways of evaluating the projection integral of Eq. (15). One can evaluate the integral directly, using the calculated $\chi(\mathbf{R}|\bar{k}_0, z_0|t)$ and $\chi(\mathbf{R}|\theta_p, \bar{k}_p, q_p)$; one can evaluate separately the partial-wave integrals $\langle \chi_l(\bar{k}_p, q_p) | \chi_l^{\text{OUT}}(\bar{k}_0, z_0|t) \rangle$, then superpose them using Eq. (41); or one can obtain the integral indirectly, from the S -matrix elements, by reversing the steps in Eqs. (41)–(44). Which route is most convenient will depend upon which numerical method has been used to solve the Schrödinger equation (see Sec. V).

E. Time-dependent S -matrix elements

As a postscript to the above, it is convenient to define the “time-dependent S -matrix” elements

$$S_l(t) = \int_0^{\infty} \frac{F(\bar{k}_0, z_0, \bar{k}_p, q_p|E)}{k} S_l(E) e^{-iEt/\hbar} dE \quad (45)$$

and the term

$$F(t) = \int_0^{\infty} \frac{F(\bar{k}_0, z_0, \bar{k}_p, q_p|E)}{k} e^{-iEt/\hbar} dE. \quad (46)$$

The expansion of $f(\theta, t)$ in Eq. (41) can then be written

$$f(\theta, t) = \frac{1}{2i} \sum_{l=0}^{\infty} (2l+1) P_l(\cos \theta) [S_l(t) - F(t)]. \quad (47)$$

Clearly, the interpretation of the $S_l(t)$ is that they are the partial-wave components of the time-dependent scattering amplitude $f(\theta, t)$. They can be calculated from the time-independent S -matrix elements $S_l(E)$, by specifying the initial and probe plane wave packets through the choice of energy filter $F(\bar{k}_0, z_0, \bar{k}_p, q_p|E)$. The term $F(t)$ subtracts the contribution of the unscattered plane wave packet $\chi^{\text{PW}}(\mathbf{R}|\bar{k}_0, z_0|t)$ from $f(\theta, t)$.

IV. NUMERICAL ILLUSTRATION

The formulas of Sec. III give a straightforward way of implementing the plane-wave scattering theory numerically. As in a coupled-channel calculation, one can calculate each partial wave separately, and truncate the series at $l=l_{\text{max}}$. Such calculations have already been done, in our previous applications of the multichannel version of the theory to chemical reactions. Here we discuss a numerical application to the simple model of scattering by a hard sphere, in order to illustrate some basic aspects of the theory. These include the form of the initial partial wave packets, the convergence of the plane wave packet with respect to l_{max} , some graphical difficulties that are encountered, and the difference between the close-up and asymptotic angular distributions.

The scattering of a particle from a hard sphere is one of the classic models of quantum scattering theory [6–8]. The partial-wave components of the wave function are known analytically, and are obtained by substituting $S_l(E)$

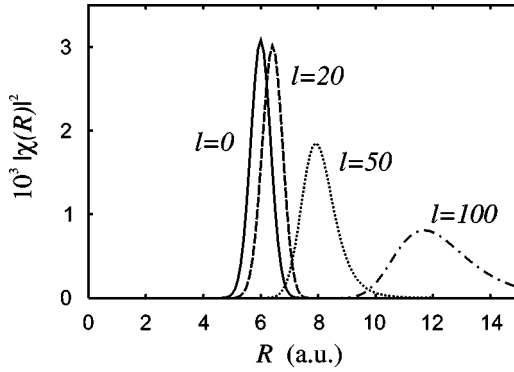


FIG. 2. Probability distributions $|\chi_l(R|\bar{k}_0, z_0|0)|^2$ obtained from selected partial wave components $\chi_l(R|\bar{k}_0, z_0|0)$ of the initial plane wave packet $\chi(\mathbf{R}|\bar{k}_0, z_0|0)$. The $\chi_l(R|\bar{k}_0, z_0|0)$ are obtained from Eq. (26), using the momentum amplitude $A(k|\bar{k}_0, z_0)$ specified in Sec. IV A.

$=\exp[2i\phi_l(k)]$ into Eq. (33), with $\phi_l(k)=\hat{j}_l(ka)/\hat{n}_l(ka)$, where a is the radius of the hard sphere. It is therefore not necessary to propagate the time-dependent wave packet numerically, since it can be obtained from $\Psi(\mathbf{R}|E)$, by reversing the steps in Eqs. (6) and (7). The same is true for the close-up and asymptotic angular distributions, which can be obtained directly from the S -matrix elements, using the equations given in Secs. III C and III D. The “numerical” aspect of the calculation therefore consists in truncating the partial-wave series at l_{\max} , and evaluating the integrals over E and k by quadrature.

A. Initial wave packets

The initial plane wave packet $\chi(\mathbf{R}|\bar{k}_0, z_0|0)$ was taken to be a Gaussian along the z coordinate. The envelope function $A(z-z_0)$ of Eq. (1) is therefore

$$A(z-z_0) = \frac{1}{\sqrt{z_l}\sqrt{\pi}} \exp\left[-\frac{(z-z_0)^2}{2z_l^2}\right]. \quad (48)$$

The initial position, width, and average momentum took the values $z_0=-6$ a.u., $z_l=0.5$ a.u., and $\bar{k}_0=10$ a.u.

The initial wave packet was expanded in terms of a series of partial wave packets $\chi_l(R|\bar{k}_0, z_0|0)$, according to Eqs. (22) and (26). To our knowledge, the integrals in Eq. (26) cannot be evaluated analytically for $l>0$, and so they were evaluated using Gauss-Hermite quadrature over k . Figure 2 plots the $|\chi_l(R|\bar{k}_0, z_0|0)|^2$ for selected values of l . As expected from the discussion in Sec. III A, the packets move further out and become wider, as l increases, this corresponding to an increasingly glancing cut through the initial plane wave packet, as the impact parameter increases.

Superposing the partial wave packets, by truncating Eq. (22) at $l=l_{\max}$, produces an approximation to the initial plane wave packet $\chi(\mathbf{R}|\bar{k}_0, z_0|0)$. Figure 3 illustrates the convergence of $\chi(\mathbf{R}|\bar{k}_0, z_0|0)$ with respect to l_{\max} . When $l_{\max}=0$, the initial wave packet is simply $\chi_0(R|\bar{k}_0, z_0|0)/R$, which is a

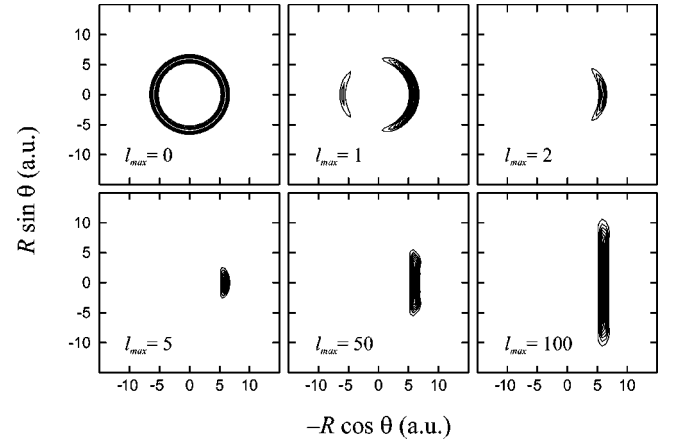


FIG. 3. Probability distributions $|\chi(\mathbf{R}|\bar{k}_0, z_0|0)|^2$ obtained by expanding the initial plane wave packet $\chi(\mathbf{R}|\bar{k}_0, z_0|0)$ using Eq. (22), and truncating the expansion at various values of $l=l_{\max}$.

Gaussian along the radial coordinate, and has a spherical distribution in the angular coordinates (θ, ϕ). Taken in isolation, this packet would give a spherical description of the scattering: the sphere in Fig. 3 would implode, reach the scattering center, then scatter spherically outwards. For $l=1, 2, \dots$ the isolated $\chi_l(R|\bar{k}_0, z_0|0)$ would give a description of the scattering that is shaped like a p orbital, d orbital, and so on.

Figure 3 shows that the effect of superposing just the first two partial waves is enough to locate most of the (approximate) plane wave packets on the negative z axis. The predominant approach direction of the packet is now along the positive z direction. As partial waves are added up to about $l_{\max}=5$, the initial plane wave packet becomes increasingly focused, concentrating into a blob about $z=z_0$. The addition of further partial waves ($l_{\max}>5$) behaves semi-classically: each additional l component widens the range of initial impact parameters, such that $\chi(\mathbf{R}|\bar{k}_0, z_0|0)$ resembles a disk (in the plane perpendicular to the z axis) of approximate radius l_{\max}/\bar{k}_0 . In a numerical calculation, l_{\max} is chosen such that the radius of the disk is just wide enough to include all the impact parameters that will scatter. If desired, the entire plane wave packet (and its subsequent time evolution) can be recovered by adding onto the wave packet the term

$$\begin{aligned} \chi^{\text{hole}}(\mathbf{R}|\bar{k}_0, z_0, l_{\max}|t) &= \chi^{\text{PW}}(\mathbf{R}|\bar{k}_0, z_0|t) \\ &\quad - \frac{1}{R} \sum_{l=0}^{l_{\max}} i^{l(2l+1)} P_l(\cos \theta) \\ &\quad \times \chi_l^{\text{PW}}(R|\bar{k}_0, z_0|t), \end{aligned} \quad (49)$$

which is the exact plane wave packet with a circular hole in it.

The probe packets $\chi(\mathbf{R}|\theta_p, \bar{k}_p, q_p)$, and their partial wave components $\chi_l(R|\bar{k}_p, q_p)$, have exactly the same forms as $\chi(\mathbf{R}|\bar{k}_0, z_0|0)$, and $\chi_l(R|\bar{k}_0, z_0|0)$, except that they are rotated by an angle of θ_p . In a numerical calculation, the probe pack-

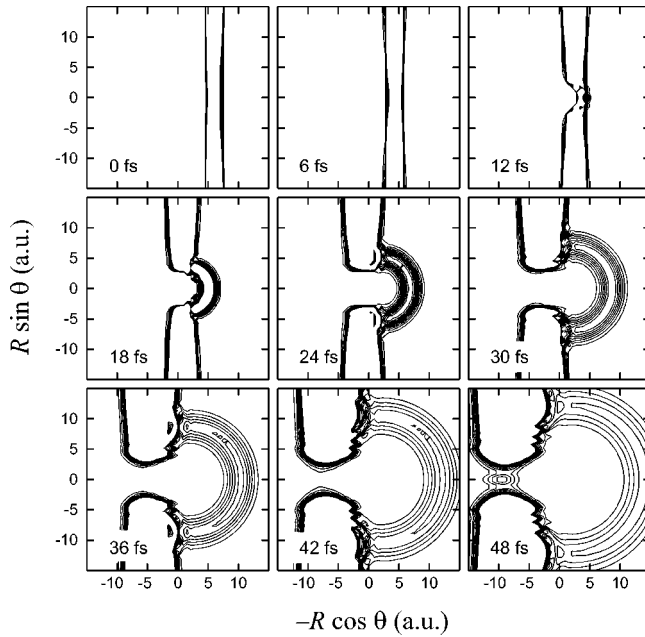


FIG. 4. Snapshots of the time-evolving probability distribution $|\chi(\mathbf{R}|\bar{k}_0, z_0|t)|^2 R^2$, showing the scattering of the plane wave packet from a hard-sphere potential, calculated as described in Sec. IV B.

ets $\chi(\mathbf{R}|\theta_p, \bar{k}_p, q_p)$ are thus disks in the plane perpendicular to the q axis. These disks have the same radius as the initial packet $\chi(\mathbf{R}|\bar{k}_0, z_0|0)$, and are therefore just wide enough to capture all of the scattered packet.

B. Time-evolving wave packets

The wave packet $\chi(\mathbf{R}|\bar{k}_0, z_0|t)$ was computed for a hard-sphere radius of $a=3.0$ a.u. The partial wave expansion was truncated at $l_{\max}=40$, which was found to be sufficient to converge the DCS over the range of collision energies contained in the initial wave packet of Eq. (48). The nonscattering part of the plane wave packet (for $l>40$) was added on using Eq. (49). The mass of the scattering particle was taken to be $m=1470$ a.u.

Figures 4 and 5 give snapshots of $|\chi(\mathbf{R}|\bar{k}_0, z_0|t)|^2 R^2$ and $|\chi^{\text{OUT}}(\mathbf{R}|\bar{k}_0, z_0|t)|^2 R^2$ at various times during the hard-sphere collision. The plots illustrate some of the graphical difficulties encountered when attempting to represent on the same plot the rectangular motion of the incoming plane wave as well as the roughly spherical evolution of the scattered wave. The latter spreads over a surface whose area scales as R^2 , and will thus quickly disappear from the plots, unless the packet is multiplied by R^2 (as is done in Figs. 4 and 5). However, the R^2 factor distorts the representation of the initial plane wave packet (which looks bent in Fig. 4). A related difficulty is that the amplitude of the unscattered part of the plane wave is much greater than the scattered part, and hence the unscattered part dwarfs the scattered part (see Fig. 4). Both difficulties are sidestepped by plotting just the scattered wave packet $|\chi^{\text{OUT}}(\mathbf{R}|\bar{k}_0, z_0|t)|^2 R^2$, as is done in Fig. 5. A convenient representation, used in some of our applications

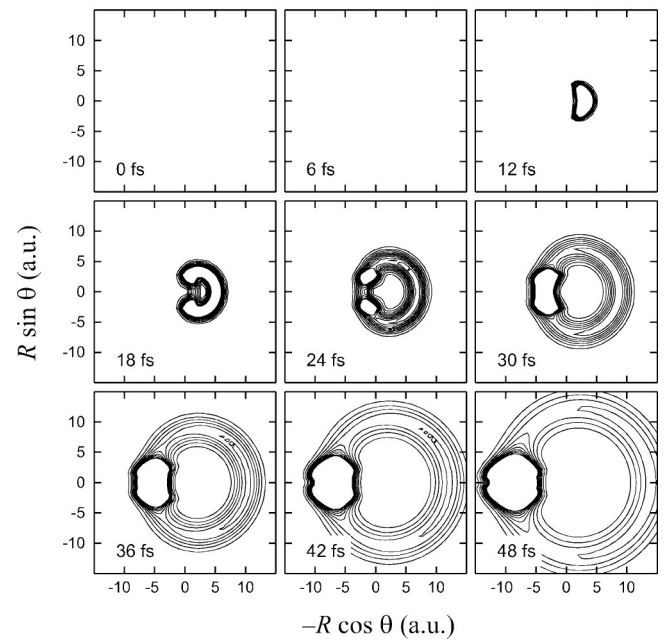


FIG. 5. Same as Fig. 4 for $|\chi^{\text{OUT}}(\mathbf{R}|\bar{k}_0, z_0|t)|^2 R^2$ (the scattered component of the wave packet).

to chemical reactions is to represent $|\chi^{\text{OUT}}(\mathbf{R}|\bar{k}_0, z_0|t)|^2$ and $|\chi^{\text{PW}}(\mathbf{R}|\bar{k}_0, z_0|t)|^2$ separately on the same plot, multiplying just $|\chi^{\text{OUT}}(\mathbf{R}|\bar{k}_0, z_0|t)|^2$ by the factor of R^2 , and using a different set of contour levels for the two functions.

There can be no surprises in Figs. 4 and 5, which represent one of the classic problems of scattering theory. The main purpose here is to illustrate the theory of Secs. II and III, in particular the relation between the the wave packet and the close-up and asymptotic angular distributions. We emphasize that in more complex systems, such as the chemical reactions we looked at previously [1–5], the wave packets often yield new insight into the dynamics of the scattering. We suggest also that, even for a simple model system such as hard-sphere scattering, the visualization given by the time-evolving wave packet may have pedagogical advantages. For example, Fig. 4 gives a clear picture, at 24 fs, of the formation of the well-known shadow. Later, at 42–48 fs, it shows how the spreading of the edges of the packet into the shadow produces the diffractive interference pattern that characterizes hard-sphere forward scattering. The scattered wave packet (Fig. 5) shows the part of the wave packet that cancels out the unscattered plane wave to generate the shadow. At 18 fs, this part appears as two surface waves, which move around the sphere and meet up in the forward direction.

C. Close-up angular distributions and DCS

The close-up, time-dependent angular distribution $\tilde{\sigma}(\theta, t)$ of Eq. (11) and the time-dependent DCS $d\sigma/d\Omega(\theta, t)$ of Eq. (16) were obtained from the S -matrix elements, using the formulas of Sec. III. For the close-up distributions, this procedure was equivalent to taking radial cuts through the wave packet as a function of θ , then projecting onto the radial

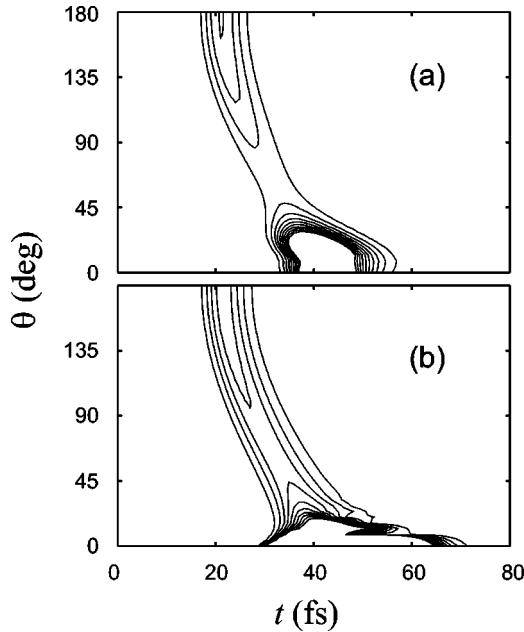


FIG. 6. Comparison of the two types of time-dependent angular distribution obtained from the scattered wave packet of Fig. 5. Panel (a) is the close-up angular distribution $\tilde{\sigma}(\theta, t)$; panel (b) is the time-dependent DCS $d\sigma/d\Omega(\theta, t)$.

probe packet $\chi_p(R|\bar{k}_p, R_p)/R$ following Eq. (10). For the asymptotic distributions, it was equivalent to projecting onto the plane wave probe packets $\chi(\mathbf{R}|\theta_p, \bar{k}_p, q_p)$ of Eq. (14). Both types of probe packets were taken to be Gaussians, centered around $R_p=6$ a.u., with the same width and average momentum as the initial packet $\chi(\mathbf{R}|\bar{k}_0, z_0|0)$ [see Eq. (48)].

The resulting $\tilde{\sigma}(\theta, t)$ and $d\sigma/d\Omega(\theta, t)$ are plotted in Fig. 6. As mentioned above, the close-up distribution $\tilde{\sigma}(\theta, t)$ is expected to give the more faithful representation of the scattering of the wave packet, since it gives the angular distribution of the packet just after it has exited the scattering potential (in this case 6 a.u. from the origin). The time-dependent DCS $d\sigma/d\Omega(\theta, t)$ is also computed at this distance, which is why the two angular distributions cover roughly the same range of t . However, one should not forget that $d\sigma/d\Omega(\theta, t)$ predicts the angle into which the packet will have scattered in the limit that $R \rightarrow \infty$.

Paradoxically, $d\sigma/d\Omega(\theta, t)$ appears to give a more faithful representation of the roughly spherical “ring” into which the packet scatters (see Fig. 5), than does the close-up distribution $\tilde{\sigma}(\theta, t)$. This is because the latter detects that the ring is not centered about the origin, but about a point on the z axis at roughly $z=-2$ a.u. The backward-scattered part of the ring has therefore traveled a shorter distance (by about 4 a.u.) than the forward-scattered part, and has spread considerably less; this has the effect of concentrating the ring in $\tilde{\sigma}(\theta, t)$ in the backward direction. By contrast, the time-dependent DCS $d\sigma/d\Omega(\theta, t)$ does not detect that the scattering is off-center. Like the time-independent DCS of conventional scattering theory, $d\sigma/d\Omega(\theta, t)$ gives the angular distribution in the limit $R \rightarrow \infty$, in which all of the scattering appears to radiate from a central point.

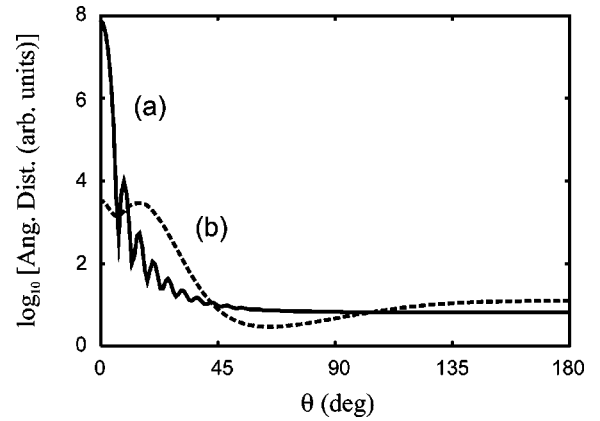


FIG. 7. A cut (at $E=1$ eV) through the time-independent angular distributions obtained from the scattered wave packet of Fig. 5. Curve (a) is the close-up angular distribution $\tilde{\sigma}(\theta, E)$; curve (b) is the time-independent DCS $d\sigma/d\Omega(\theta, E)$. The curves have been scaled to fit on the same plot.

Another difference between $\tilde{\sigma}(\theta, t)$ and $d\sigma/d\Omega(\theta, t)$ is evident in the forward direction, where $d\sigma/d\Omega(\theta, t)$ shows a narrowly focused forward peak, which contains oscillations in θ caused by the diffractive interference. In $\tilde{\sigma}(\theta, t)$, the forward peak spreads over a wider range of angles, and does not contain the diffractive oscillations. This is because $\tilde{\sigma}(\theta, t)$ detects the packet where it has just emerged from colliding with the hard sphere, and where the two edges of the forward-scattering packet have not yet come together and interfered. Hence, $\tilde{\sigma}(\theta, t)$ shows that the forward interference is caused, not by the dynamics of the packet as it hits the sphere, but later, as the particle scatters outwards. This very well-known example illustrates how the time-dependent angular distributions $\tilde{\sigma}(\theta, t)$ and $d\sigma/d\Omega(\theta, t)$ complement one another.

Figure 7 shows the close-up, time-independent angular distribution $\tilde{\sigma}(\theta, E)$, and the time-independent DCS $d\sigma/d\Omega(\theta, E)$, at $E=1$ eV. The forward scattering region ($\theta=0-45^\circ$) illustrates clearly the diffractive oscillations, which as just discussed, are not present in the close-up distribution.

Together, the four angular distributions, $\tilde{\sigma}(\theta, t)$, $d\sigma/d\Omega(\theta, t)$, $\tilde{\sigma}(\theta, E)$, and $d\sigma/d\Omega(\theta, E)$ summarize the dynamics of the wave packet shown in Figs. 4 and 5. In particular, the time-dependent DCS $d\sigma/d\Omega(\theta, t)$ illustrates which parts of the wave packet map onto which parts of the DCS. In this simple example, the mapping is obvious, since we know that the earlier parts of the packet scatter in the backward direction, and so on. However, in more complex systems, such as chemical reactions [1–5], the time-dependent DCS is very useful at disentangling contributions from different scattering mechanisms.

V. APPLYING THE THEORY IN TIME-INDEPENDENT CALCULATIONS

The theory of Secs. II and III uses wave packets as an interpretational tool, for visualizing collisions and interpreting the DCS. This use of wave packets should not be con-

TABLE I. Summary of the extent to which different types of time-independent (TI) scattering calculation can make use of the plane wave packet theory of this paper—see Sec. V.

TI calculation yields	$\chi(t)$	$\bar{\sigma}(\theta, E)$	$\bar{\sigma}(\theta, t)$	$d\sigma/d\Omega(\theta, t)$	$S_l(t)$
$\Psi(E)$ and $f(\theta, E)$ over grid of E	✓	✓	✓	✓	✓
$f(\theta, E)$ over grid of E	×	✓	✓	✓	✓
$S_l(E)$ for some l over grid of E	×	×	×	×	✓
$f(\theta, E)$ for some values of E	×	✓	×	×	×

fused with the other use of wave packets in quantum scattering, which is a numerical method of solving the Schrödinger equation [11–17]. It seems natural to use the latter method in combination with the theory of Secs. II and III, since an existing time-dependent code can easily be modified to propagate the (multichannel equivalent of) the initial partial wave packets $\chi_l(R|\bar{k}_0, z_0|0)$ of Eq. (26). However, we emphasize that the theory of Secs. II and III is also applicable when the Schrödinger equation is solved using a time-independent method, such as the coupled-channel [21] or R -matrix [22] method. One has simply to compute the time-independent wave function $\Psi(\mathbf{R}|E)$ and scattering amplitude $f(\theta, E)$ over a grid of energies, then reverse the steps in Eqs. (6), (7), (17), and (18). This was how we calculated the hard-sphere results of Sec. IV.

In fact, the latter approach has the advantage that it may be repeated any number of times, using different choices of the energy filter $F(\bar{k}_0, z_0, \bar{k}_p, q_p|E)$. One may therefore obtain time-evolving wave packets and angular distributions from $\Psi(\mathbf{R}|E)$ that explore different energy ranges, impact parameters, and initial conditions. Hence, it can even make sense, when solving the Schrödinger equation by time-dependent methods, to Fourier-transform the wave packet to the energy-domain, to obtain $\Psi(\mathbf{R}|E)$ and $f(\theta, E)$ over a grid of E . One can then Fourier transform back to the time domain, using a variety of different $F(\bar{k}_0, z_0, \bar{k}_p, q_p|E)$. This was the approach used in Ref. [4] [where different $F(\bar{k}_0, z_0, \bar{k}_p, q_p|E)$ were used to isolate and focus a particular scattering mechanism].

Of course, there are many examples of time-independent calculations in which it is not practical to calculate the wave function and S -matrix elements over a grid of E , and over all the partial waves required to converge $f(\theta, E)$. The extent to which the theory of Secs. II and III can be applied to interpret the results obtained from less comprehensive time-independent calculations is summarized in Table I.

VI. CONCLUSIONS

This paper has derived the plane wave packet approach to quantum scattering which was applied previously (on the basis of physical intuition) to chemically reactive scattering. The derivation shows that there is a simple, rigorous mapping between a wave packet that is initiated and detected close to the scattering potential, and the DCS (which is measured a large distance away from the potential). The mapping can be illustrated graphically by means of a “time-dependent DCS.” In addition, the evolution of the packet as it exits the

potential can be summarized by means of close-up time-dependent and time-independent angular distributions.

The approach is a simple idea, but it has turned out to be a powerful tool for interpreting the cross sections of chemical reactions [1–5]. These are systems in which the DCS is complicated by interference patterns between competing scattering processes, which the plane wave packet approach is able to disentangle neatly. An advantage with treating chemical reactions is that their dynamics is usually semiclassical [23–26], and is thus described naturally by localized wave packets (just as unimolecular processes are described naturally by wave packets prepared in “femtochemistry” experiments [27]). It will be interesting, therefore, to see whether the approach of this paper can also interpret the dynamics of other systems which have competing scattering mechanisms, but which are not semiclassical (e.g., electron-molecule scattering [22]).

The derivation in this paper was restricted to the simplest case of spherical-particle scattering, in order to illustrate and prove the key ideas (such as the mapping between the wave packet and the DCS, and the differences between the various angular distributions). It is easy to extend this derivation to multichannel scattering, and this will be published shortly. So far, we have restricted our derivation and applications of the approach to systems in which the scattering potential has a finite range. Extending the approach to treat systems with infinite-range potentials should be straightforward (e.g., in charged-particle scattering, the initial and probe plane wave packets would be superpositions of Coulomb functions [6–8]). It may also be possible (although we have not explored this possibility) to extend the approach to scattering in the presence of external fields.

ACKNOWLEDGMENTS

It is a pleasure to thank Dr. Stephen Gray (Argonne) for pointing out the analogies with electromagnetic wave scattering and suggesting Refs. [9,10]. I also thank Professor J.N.L. Connor (Manchester) for checking through the manuscript and making suggestions. Finally, I acknowledge the Royal Society for support.

APPENDIX A

To prove Eq. (7), we follow Ref. [18], which proves the analogous relation for the case of one-dimensional (1D) scattering. First, we give the formal expression for $\xi(\mathbf{R}|\bar{k}_0, z_0|E)$, which is

$$\xi(\mathbf{R}|\bar{k}_0, z_0|E) = \lim_{\epsilon \rightarrow 0^+} \frac{1}{2\pi\hbar} \int_0^\infty e^{-i(\hat{H} - i\epsilon - E)t/\hbar} dt \chi(\mathbf{R}|\bar{k}_0, z_0|0), \quad (\text{A1})$$

where the factor $\exp(-\epsilon t)$ ensures that the integral converges at large t . We can rewrite this schematically as

$$\xi = \frac{i}{2\pi} G \chi(0), \quad (\text{A2})$$

recognizing that the integral over t is the Green's function G corresponding to outgoing wave boundary conditions [6–8]. In this notation, G satisfies the Lippmann-Schwinger equation [6–8]

$$G = G^{\text{PW}} + GVG^{\text{PW}}, \quad (\text{A3})$$

where V represents, schematically, the scattering potential, and G^{PW} is the Green's function for the free particle (i.e., with \hat{H} replaced by \hat{H}_0). We then have that

$$\xi = \xi^{\text{PW}} + GV\xi^{\text{PW}}, \quad (\text{A4})$$

where

$$\xi^{\text{PW}} = \frac{i}{2\pi} G^{\text{PW}} \chi(0). \quad (\text{A5})$$

Now, Eq. (A4) resembles the Lippmann-Schwinger equation for the time-independent wave function $\Psi(\mathbf{R}|E)$:

$$\Psi = \Psi^{\text{PW}} + GV\Psi^{\text{PW}}, \quad (\text{A6})$$

where $\Psi^{\text{PW}} = \exp(ikz)$. Hence, to prove Eq. (7) we have only to show (reverting to the full notation) that

$$\xi^{\text{PW}}(\mathbf{R}|\bar{k}_0, z_0|E) = \frac{mA(k|\bar{k}_0, z_0)}{\hbar^2 k} e^{ikz}. \quad (\text{A7})$$

If we replace \hat{H} in Eq. (A1) by \hat{H}_0 , and write out $\hat{H}_0 = \hat{T}_x + \hat{T}_y + \hat{T}_z$ [where $\hat{T}_x = -\hbar^2/(2m)d^2/dx^2$, etc.], then it is evident that

$$\xi^{\text{PW}}(\mathbf{R}|\bar{k}_0, z_0|E) = \lim_{\epsilon \rightarrow 0^+} \frac{1}{2\pi\hbar} \int_0^\infty e^{-i(\hat{T}_z - i\epsilon - E)t/\hbar} dt A(z - z_0) e^{i\bar{k}_0 z}, \quad (\text{A8})$$

which reduces the problem to the 1D system treated in Ref. [18]. The latter showed that the right-hand side of Eq. (A8) is equal to the right-hand side of Eq. (A7), except for those components of $\Psi(z|E)$ which are produced by the $t < 0$ parts of the wave packet [i.e., the incoming wave, $\exp(ikz)$, for $z < z_0$]. Hence, we have proved that Eq. (7) is satisfied, except for the incoming wave component of $\Psi(\mathbf{R}|E)$, for $z < z_0$.

APPENDIX B

To evaluate the integral in Eq. (43), we use a result of Ref. [18], which is that, for a general choice of initial partial wave packet $\chi_l(R|0)$, the partial-wave TIWP $\xi_l(R|E)$ is related to $\Psi_l(R|E)$ by

$$\xi_l(R|E) = \frac{-2mi}{k\hbar^2} B_l^+(k) \Psi_l(R|E), \quad (\text{B1})$$

where

$$B_l^+(k) = \frac{1}{2\pi} \int_0^\infty \chi_l(R|0) \hat{h}_l^+(kR) dR. \quad (\text{B2})$$

In the plane wave packet approach of this paper, the initial wave packet has the specific form $\chi_l(R|0) = \chi_l(R|\bar{k}_0, z_0|0)$, where $\chi_l(R|\bar{k}_0, z_0|0)$ is given in Eq. (26). In this case, the TIWP $\xi_l(R|\bar{k}_0, z_0|E)$ is also related to $\Psi_l(R|E)$ by Eq. (32). Comparing the latter with Eq. (B1) shows that, when $\chi_l(R|0) = \chi_l(R|\bar{k}_0, z_0|0)$,

$$B_l^+(k) = \frac{iA(k|\bar{k}_0, z_0)}{2k}. \quad (\text{B3})$$

Hence, from Eq. (B2), we see that the integral in Eq. (43) is equal to $i\pi A(k|\bar{k}_p, q_p)/k$.

-
- [1] S. C. Althorpe, F. Fernández-Alonso, B. D. Bean, J. D. Ayers, A. E. Pomerantz, R. N. Zare, and E. Wrede, *Nature (London)* **416**, 67 (2002).
- [2] S. C. Althorpe, *J. Chem. Phys.* **117**, 4623 (2002).
- [3] S. C. Althorpe, *Chem. Phys. Lett.* **370**, 443 (2003).
- [4] S. C. Althorpe, *J. Phys. Chem. A* **107**, 7152 (2003).
- [5] J. C. Juanes-Marcos and S. C. Althorpe, *Chem. Phys. Lett.* **381**, 743 (2003).
- [6] M. L. Goldberger and K. M. Watson, *Collision Theory* (Wiley, New York, 1964).
- [7] R. G. Newton, *Scattering Theory of Waves and Particles* (Springer-Verlag, New York, 1982).
- [8] C. J. Joachain, *Quantum Collision Theory* (Elsevier, Amsterdam, 1983).
- [9] A. Taflove and K. R. Umashankar, *IEEE Trans. Electromagn. Compat.* **25**, 433 (1983).
- [10] A. Taflove and S. C. Hagness, *Computational Electrodynamics: The Finite-Difference Time-Domain Method* (Artech House, Boston, 2000), Chap. 8.
- [11] D. Neuhauser, M. Baer, R. S. Judson, and D. J. Kouri, *J. Chem. Phys.* **90**, 5882 (1989).
- [12] S. C. Althorpe, *J. Chem. Phys.* **114**, 1601 (2001).
- [13] T. Peng and J. Z. H. Zhang, *J. Chem. Phys.* **105**, 6072 (1996).
- [14] D. H. Zhang, M. A. Collins, and S.-Y. Lee, *Science* **290**, 961 (2000).
- [15] S. K. Gray and G. G. Balint-Kurti, *J. Chem. Phys.* **108**, 950 (1998).
- [16] A. J. H. M. Meijer and E. M. Goldfield, *J. Chem. Phys.* **110**, 870 (1999).
- [17] M. Lara, A. Aguado, M. Paniagua, and O. Roncero, *J. Chem.*

- Phys. **113**, 1781 (2000).
- [18] D. J. Kouri and D. K. Hoffman, *Few-Body Syst.* **18**, 203 (1995).
- [19] D. J. Kouri, Y. Huang, W. Zhu, and D. K. Hoffman, *J. Chem. Phys.* **100**, 3662 (1994).
- [20] The units of $d\sigma/d\Omega(\theta, t)$ depend on the units of the momentum amplitudes $A(k|\bar{k}_0, z_0)$ and $A(k|\bar{k}_p, q_p)$. Only if these are chosen to be dimensionless are the units of $d\sigma/d\Omega(\theta, t)$ those of area.
- [21] D. Skouteris, J. F. Castillo, and D. E. Manolopoulos, *Comput. Phys. Commun.* **133**, 128 (2000).
- [22] I. Rozum, N. J. Mason, and J. Tennyson, *J. Phys. B* **36**, 2419 (2003).
- [23] M. S. Child, *Semiclassical Mechanics with Molecular Applications* (Clarendon, Oxford, 1991).
- [24] A. J. Dobbyn, P. McCabe, J. N. L. Connor, and J. F. Castillo, *Phys. Chem. Chem. Phys.* **1**, 1115 (1999).
- [25] W. H. Miller, *J. Phys. Chem. A* **105**, 2942 (2001).
- [26] F. J. Aoiz, L. Bañares, and V. J. Herrero, *J. Chem. Soc., Faraday Trans.* **94**, 2483 (1998).
- [27] *Femtochemistry and Femtobiology: Ultrafast Dynamics in Molecular Science*, edited by A. Douhal and J. Santamaria (World Scientific, Singapore, 2002).